Photogrammetry Assisted Rapid Measurement of Earthquake-Induced Building Damage

Fei Dai, PhD
Hong Kong Polytechnic University
cefdai@polyu.edu.hk and sites.google.com/site/cedaif

Suyang Dong, PhD Candidate
University of Michigan
dsuyang@umich.edu

Vineet R. Kamat, Associate Professor
University of Michigan
vkamat@umich.edu and pathfinder.engin.umich.edu

Ming Lu, Associate Professor
University of Alberta
mlu6@ualberta.ca

ABSTRACT: *The presented research investigates the application of close-range photogrammetry surveying techniques and Augmented Reality (AR) visualization to design a semi-automated method for rapidly measuring structural damage induced in tall buildings by seismic events such as earthquakes or explosions. Close-range photogrammetry algorithms were designed to extract spatial information from photographic image data, and geometrically measure the horizontal drift (also called Inter-Storey Drift) sustained at key floors along the edge of a damaged building. The measured drift can then be used to compute damage indices that correlate the drift to the building's structural integrity and safety. In this research, the measurement accuracy of the calculated drift using photogrammetry is particularly studied. The experimental results revealed an accuracy level of 5 mm, demonstrating the potential of photogrammetry assisted rapid measurement of earthquake-induced building damage.*

KEYWORDS*: Buildings, Damage, Earthquakes, Reconnaissance, Computer applications, Photogrammetry*

1. INTRODUCTION

Timely and accurate evaluation of damage sustained by buildings after seismic events such as earthquakes or explosions is critical to determining the building's safety and suitability for their future occupancy. Time used in conducting the evaluations substantially affects the duration for which the potentially damaged buildings remain unusable. The elapsed time may lead to direct economic losses to both public societies and private owners. Current practice of evaluating the damage to buildings mainly resorts to licensed inspectors manually inspecting the building's integrity and habitability based on their personal experience and knowledge. Though inspection guidelines exist (for example, contained in the ATC-20 1989 and ATC-20-2 1995), the work of manual inspection remains labor-intensive and time-consuming, and the results are subjective and can often be error-prone (Kamat and El-Tawil 2007).

The presented research makes an attempt to alleviate this situation. By investigating the application of close-range photogrammetry surveying techniques and Augmented Reality (AR) visualization, a semi-automated method is designed to rapidly measure the structural damage induced in tall buildings by seismic events such as earthquakes or explosions. Close-range photogrammetry algorithms are designed to extract spatial information from photographic image data, and geometrically measure the horizontal drift (also called Inter-Storey Drift) sustained at key floors along the edge of a damaged building. The measured drift can then be used to compute damage indices that correlate the drift to the building's structural integrity and safety.

In this research, vision-based AR techniques identify the pixel positions of key points along a building's edge in photographs, and close-range photogrammetry computes the 3D coordinates of those points into the global object space, considering only the drift component that is perpendicular to the direction of the camera's line of sight. The inter-storey drift can be subsequently derived by comparing the shifted position of each floor against the pre-disaster outer geometry of the inspected building that is obtained or available a-priori from building owner or

government databases. The Global Positioning System (GPS) and 3D electronic compasses are used to track the position and orientation of the camera's perspective.

Studying the measurement accuracy of the calculated drift using photogrammetry has been a primary focus of this research. Theoretically, components that account for measurement error mainly comprise the internal errors induced by the camera lens distortion, calculated approximation of the principal distance, the combination of the camera resolution, shooting distance and the focal length, and the external errors transferred from the tracking systems utilized to obtain the camera position and angular orientation. This research models the internal errors as mathematical formulations and correspondingly proposes solutions to minimize those errors. In order to quantitatively assess the level of accuracy, three groups of laboratory experiments were conducted to simulate a building damaged in an earthquake. A two-storey reconfigurable steel frame was designed to resemble a building structure. The frame was calibrated with known displacement values at the second floor, and images were taken with a Canon EOS Rebel T1i digital camera. The images were post-processed to yield the spatial coordinates of two bolted connections on each of the frame's two floors. By subtracting horizontal axis components of the two connections, the inter-storey drift was computed. The experimental results revealed an accuracy level of 5 mm, demonstrating the potential of photogrammetry assisted rapid measurement of earthquake-induced building damage.

The remainder of this paper elaborates on the photogrammetry assisted methodology in detail, followed by the analytical study of the internal components of cameras that induce the measurement errors, based on which the solution to minimize those errors is proposed. Finally, the laboratory experiments conducted to validate the level of measurement accuracy by photogrammetry are described, followed by a description of ongoing work toward full automation of the proposed method.

2. METHODOLOGY FOR RAPIDLY MEASURING BUILDING DAMAGE INDUCED BY EARTHQUAKE

2.1 Previous work

This study builds on prior research conducted at the University of Michigan. Previous research (Kamat and El-Tawil 2007) established a schematic overview of a rapid, augmented reality based, post-earthquake building damage reconnaissance method. As shown in Fig. 1, the previously established reconnaissance methodology utilized the augmented reality visualization techniques to superimpose the building's pre-earthquake geometric outer lines onto the view of the actual structure captured in real time through a video camera in an AR setting. The methodology proposed that equipped with a GPS receiver and 3D electronic compasses to track the position and orientation of the observer's perspective, the in-situ reconnaissance inspectors see through a head-mounted display to qualitatively evaluate the damage by comparing two views of the structure in a real time.

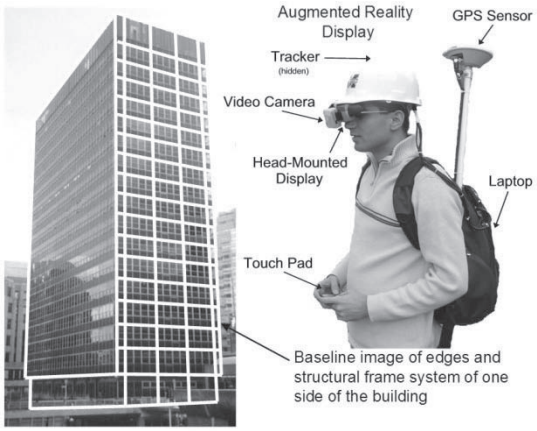

Fig. 1: Overview of previously established reconnaissance methodology (Kamat and El-Tawil 2007)

Some proof-of-concept experiments were conducted to achieve a quantitative result in the previous research. In the UM Structural Engineering Laboratory, the large-scale cyclic shear walls were selected as the test-bed and the CAD images of the walls were overlaid onto the actual wall specimens. As loading was applied on the wall specimens, the displaced horizontal drifts were measured by placing the baselines of the CAD images in the augmented space and comparing the baselines with the edges of the actual wall specimens. The experimentally

measured drifts were compared with the actual wall drifts quantified in a predetermined displacement regime. The results indicated a promising potential of applying AR for rapid building damage detection (Kamat and El-Tawil 2007).

Though AR visualization techniques work well in laboratory environments, some hurdles must be addressed before AR can be implemented in a field-deployable system, one of which is that the line of sight of the inspector (video camera) must be exactly orthogonal to the floors of the inspected building such that the trigonometry calculation can be applied to infer the deformed drifts (Fig. 2a). Any oblique, even slightly, line of sight to the floors of the inspected structure will lead to non-linear, biased drifts that fail to represent the actual drift measurements (Fig. 2b). Successfully applying AR techniques to measure the building damage largely depends on the standing point and viewing perspective where the inspector observes the structure. However, in potentially chaotic disaster scenarios, the inspectors who wear the reconnaissance systems can, at best, find it challenging to intuitively fine-tune their perspective to achieve the desired perpendicularity, thereby limiting the widespread use of AR visualization technology for post-earthquake reconnaissance in reality.

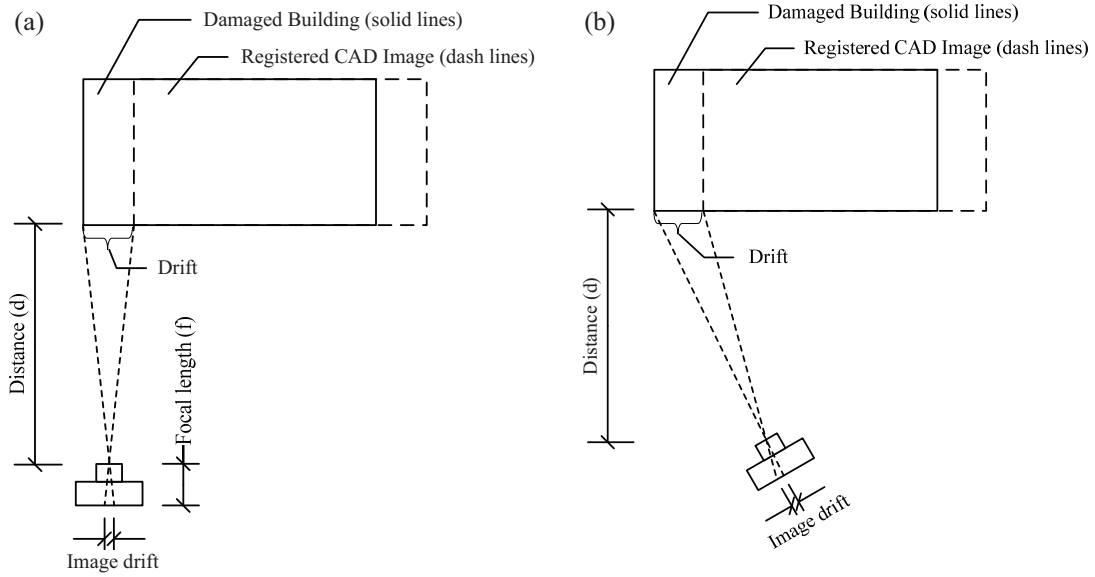

Fig. 2: Camera line of sight (a) orthogonal to building wall to derive the damage drift, but (b) oblique resulting in a non-linear, biased drift

The surveying technique of close-range photogrammetry is powered with capacity of spatialized computation and is capable of establishing a relationship between two-dimensional (2D) photo images and the three-dimensional (3D) object space (Blachut and Burkhardt 1989). Using photogrammetry allows for the inspectors to observe the structure at a standing point and viewing perspective that does not impose orthogonality, thereby complementing AR well in manipulating image data into 3D coordinates and extrapolating the inter-storey drifts. In the next section, the close-range photogrammetry technique is meticulously investigated in order to design a practical and universal AR-based method for rapid post-earthquake building damage reconnaissance.

2.2 Photogrammetry assisted damage measurement

Photogrammetry is employed mainly to quantify the spatial coordinates of each floor of the damaged building. The vision-based AR technology is used to identify and extract x, y positions of building floors on the captured images. Then the x, y position data is used as the input for post processing of the photogrammetry to derive the corresponding spatial coordinates X, Y, and Z readily for the computation of the *Inter-Storey Drift* sustained at key floors along the edge of a damaged building.

In the earthquake engineering community, based on the performance-based seismic design specifications such as FEMA (2000), the *Inter-Storey Drift* (*ISD*) is used to compute indices that are unanimously suggested as a reasonable measure to reflect the extent of a building damage induced by earthquake. The *Inter-Storey Drift* can be interpreted as the horizontal displacement of each building floor that is permanently moved relative to the one beneath in regard to the damaged building. Fig. 3 illustrates the inter-storey drifts using a simplified two-storey building frame. In Fig. 3, the building frame drawn by solid lines denotes the geometric building profile pre

earthquake and the one drawn by dash curves represents the building's inclined outer walls post earthquake. From Fig. 3, the inter-storey drift of the first storey is the horizontal movement of the second floor (L_2) relative to the ground floor (L_1) which is denoted by Drift_1 (Fig. 3), and the inter-storey drift of the second storey (Drift_2 in Fig. 3) is that of the third floor (L_3) relative to the second floor (L_2) instead of the ground floor.

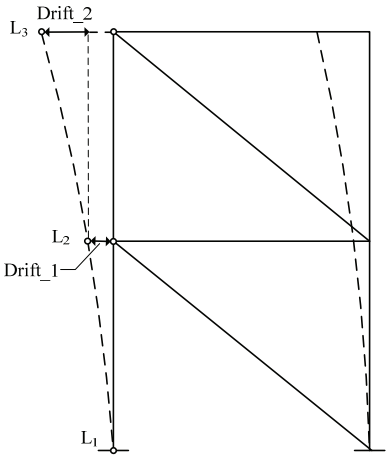

Fig. 3: A simple two-storey building frame illustrating inter-storey drifts

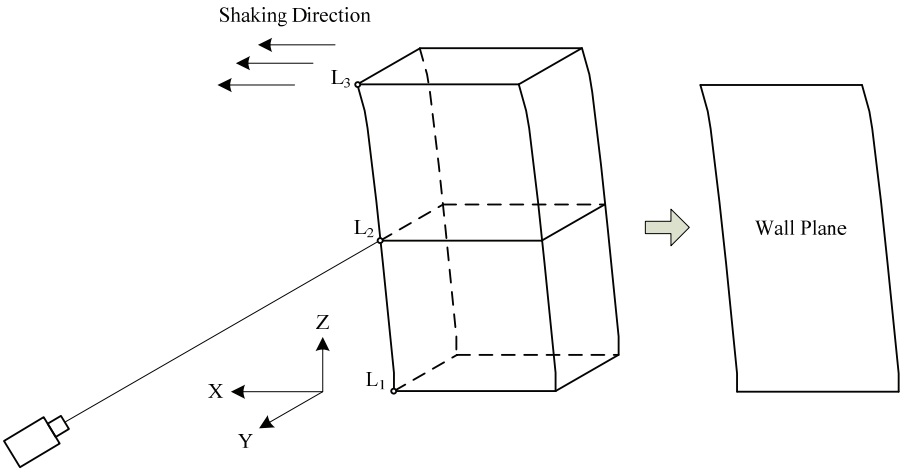

Fig. 4: An inspector inspecting the damaged building, focusing on one of the key floors at certain moment (e.g., the second floor)

The two-storey reconfigurable building frame constructed by the authors, and described earlier, will be used to demonstrate the computing algorithm for the inter-storey drift for each of the building floors, in which the 3D coordinates of the inspected floors of the damaged building should be derived first. Fig. 4 models an inspector inspecting the damaged building, focusing on one of the key floors at a certain moment (e.g., the second floor). The inspector is simply modeled by a video camera that is mounted on the inspector's helmet to capture the images of the structural damage sustained by the building. The video camera and the inspector have the same position and orientation when the building is viewed. A line of sight of the video camera is formed to link the point of the floor intersecting the building edge (e.g., L_2) in the global space with its corresponding projection on the captured image inside the camera. We denote the floor along the building edge (e.g., L_2) as its 3D coordinates in the object coordinate system of the global space (X_n, Y_n, Z_n) and its 2D coordinates on the image plane inside the camera (x_n, y_n). Thus, the line of sight can be modeled by the well-known photogrammetric *collinearity equations* (Wong 1980; Wolf 1983; McGlone 1989), as in Eq. (1):

$$x_n - x_p = -c\frac{m_{11}(X_n - X_c) + m_{12}(Y_n - Y_c) + m_{13}(Z_n - Z_c)}{m_{31}(X_n - X_c) + m_{32}(Y_n - Y_c) + m_{33}(Z_n - Z_c)}$$
$$y_n - y_p = -c\frac{m_{21}(X_n - X_c) + m_{22}(Y_n - Y_c) + m_{23}(Z_n - Z_c)}{m_{31}(X_n - X_c) + m_{32}(Y_n - Y_c) + m_{33}(Z_n - Z_c)} \quad (1)$$

In Eq. (1), (x_p, y_p) is the *principal point* on the image plane and c is the *principal distance*. They describe the internal orientation of the camera station, which can be referred to as the projected position of the light ray on the image plane through center of the lens opening of the camera (perspective center) from infinity (*principal point*), and the perpendicular distance between the perspective center and the image plane (*principal distance*). The camera internal components can be determined by performing the camera calibration, which will be described in the ensuing section entitled "Camera Calibration". Eq. (1) also has (X_c, Y_c, Z_c) and m_{ij} (i, j = 1, 2, 3) to define the exterior orientation of the camera station. (X_c, Y_c, Z_c) refer to the position of the perspective center and m_{ij} are the elements of an rotation matrix M, which are expressed as functions of the Euler orientation angles - azimuth (α), tilt (t), and swing (s) (Wolf 1983), as elaborated in Eq. (2):

$$\begin{aligned}
m_{11} &= -\cos\alpha\cos s - \sin\alpha\cos t\sin s \\
m_{12} &= \sin\alpha\cos s - \cos\alpha\cos t\sin s \\
m_{13} &= -\sin t\sin s \\
m_{21} &= \cos\alpha\sin s - \sin\alpha\cos t\cos s \\
m_{22} &= -\sin\alpha\sin s - \cos\alpha\cos t\cos s \\
m_{23} &= -\sin t\cos s \\
m_{31} &= -\sin\alpha\sin t \\
m_{32} &= -\cos\alpha\sin t \\
m_{33} &= \cos t
\end{aligned} \quad (2)$$

However, only one line of sight (Eq. 1) is not sufficient to determine the position of the inspected floor where it intersects the vertical edge of the building wall (i.e. two equations fail to solve for three unknowns.) One more extra component as a constraint is required in order to define a third equation.

In seismic engineering, it is mainly the destructive forces of an earthquake coming along the horizontal direction that induce structural damage in buildings. To simplify the problem in this research, the inspected floors' deformation is assumed to take place only on the walls whose axes are parallel or close to the shaking direction of the seismic forces (Fig. 4), leading to which the deformed floors remain in a plane that is unchanged pre and post earthquake as shown in Fig. 4. The wall plane thus can serve as the extra component constraint for the line of sight, as modeled in Eq. (3):

$$AX_n + BY_n + C = 0 \quad (3)$$

Note that the wall plane is vertical to the ground such that the variable Z_n along Z-axis is not necessary for Eq. (3). The A, B, and C are the coefficients of the equation denoting the wall plane, which can be referred to from the pre-disaster outer geometry of the inspected building that is obtained or available a-priori from the building owner or government databases.

Using the line of sight formula Eq. (1) and the plane equation Eq. (3) where the wall deforms along the shaking direction, the coordinates (X_n, Y_n, Z_n) of the inspected floor along the building edge can be finally computed. Simply denoting (X_u, Y_u, Z_u) as the edge position of the inspected floor and (X_l, Y_l, Z_l) as that of the floor beneath, the inter-storey drift (*ISD*) of the inspected floor can be subsequently computed by Eq. (4), as per:

$$ISD = (X_u - X_l)/|X_u - X_l|\sqrt{(X_u - X_l)^2 + (Y_u - Y_l)^2} \quad (4)$$

where $(X_u - X_l)/|X_u - X_l|$ indicates direction of the inspected floor's movement, i.e. plus (+): along the X-axis,

minus (-): against the X-axis, and $\sqrt{(X_u - X_l)^2 + (Y_u - Y_l)^2}$ calculates the absolute value of the movement.

Applying the photogrammetry assisted computing equations also needs the camera station' external components (X_c, Y_c, Z_c, α, t, s) and internal components (x_n, y_n, c) to be determined in advance so as to fit the parameters of the *collinearity equations* (Eq. 1), which will be discussed in the following sections.

3. MEASURING CAMERA POSITION AND ORIENTATION

The camera station's spatial coordinates (X_c, Y_c, Z_c) and orientation angles (α, t, s) are traditionally determined by means of identifying corresponding points on multiple images taken from different perspectives and fixing absolute position of camera by use of known reference points, giving rise to a lack of the ease of operation and applicability. In this research, we employ the Real Time Kinematics Global Positioning System (RTK-GPS) and a 3D electronic compass to measure the (X_c, Y_c, Z_c) and (α, t, s) of the camera's perspective respectively, which enables a maximal degree of freedom for the proposed method applied in the outdoor environment. The RTK-GPS applied is the Trimble Ag GPS Base Station 900 with a horizontal accuracy of 1-2 ppm (parts-per-million) and vertical accuracy of 2-3 ppm (parts-per-million), namely, if the distance (baseline length) between the base station and the rover receiver is 10 km, the horizontal error of the RTK-GPS is 10 - 20 mm and its vertical error is 20 - 30 mm. The 3D electronic compass is the PNI TCM 5 which uses the rotation definition of flight dynamics as per: -90º ~ 90º in pitch, -180º ~ 180º in roll, and -180º ~ 180º in heading (yaw), and has a level of rotation accuracy of 0.3°. The mapping between the flight dynamics rotation angles and the photogrammetry tilted rotation angles for Earth Axes is as: azimuth (α) = heading, tilt (t) = 90º + pitch, and swing (s) = 180º - roll, if pitch ≤ 0º; and azimuth (α) = 180º + heading, tilt (t) = 90º + pitch, and swing (s) = 180º - roll, if pitch > 0º.

4. EVALUATING CAMERA'S SYSTEMATICAL ERROR

Camera systematical error refers to the measurement error on the image plane induced by the imperfection of the camera lens and its internal mechanics with a consistent effect that cannot be statistically eliminated (Viswanathan 2005). In this section, we discuss two major aspects that induce the camera's systematical error, namely – the lens distortion and the approximation of the principal distance.

4.1 Lens Distortion

In an ideal situation, a spatial point P is projected through a camera lens opening (O) on the image plane to have an image point p, and the three points P, O, and p lie along a straight line (Fig. 5). But in reality owing to the lens distortion of the camera, the projected image point is shifted from its true p (x_n, y_n) to a disturbed position p'(x_n', y_n') as illustrated in Fig. 5, resulting in an offset between the two positions. Denoting the offset by dx and dy, thus the true coordinates of any image point can be compensated by Eq. (5):

$$\begin{aligned} x_n &= x_n^{'} + dx \\ y_n &= y_n^{'} + dy \end{aligned} \tag{5}$$

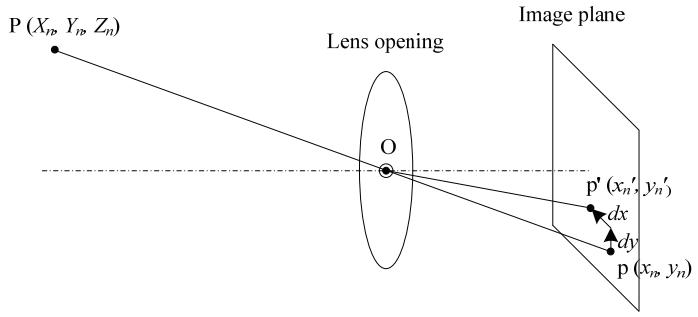

Fig. 5: Camera lens distortion inducing an offset between true and disturbed positions of a point on the image plane

For modern digital cameras, the camera lens distortion (i.e. dx and dy) can be taken as the aggregate of the radial distortion and the decentering distortion (Beyer et al. 1995; Fraser 1996). As the lens of a camera is actually composed of a combination of lenses, the centers of those lens elements are not strictly collinear, giving rise to the decentering distortion. In contrast, the radial distortion occurs in each single optical lens and the distortion effect is

magnified along the radial direction of the lens: the further a point is away from the center of the lens, the larger error is produced for its projected image point. Therefore, *dx*, *dy* can be decomposed by Eq. (6):

$$\begin{aligned} dx &= dx_r + dx_d \\ dy &= dy_r + dy_d \end{aligned} \tag{6}$$

in which dx_r , dy_r is the radial distortion along x-axis, and y-axis; and dx_d , dy_d is the decentering distortion along x-axis, and y-axis. Assuming the optical axis of the lens is perpendicular to the image plane, Brown (1966) developed the mathematical model for correcting the lens distortion by Eq. (7):

$$\begin{aligned} dx_r &= K_1(x_n^{'} - x_p)r^2 + K_2(x_n^{'} - x_p)r^4 + K_3(x_n^{'} - x_p)r^6 \\ dy_r &= K_1(y_n^{'} - y_p)r^2 + K_2(y_n^{'} - y_p)r^4 + K_3(y_n^{'} - y_p)r^6 \\ dx_d &= P_1[r^2 + 2(x_n^{'} - x_p)^2] + 2P_2(x_n^{'} - x_p)(y_n^{'} - y_p) \\ dy_d &= P_2[r^2 + 2(y_n^{'} - y_p)^2] + 2P_1(x_n^{'} - x_p)(y_n^{'} - y_p) \\ r^2 &= (x_n^{'} - x_p)^2 + (y_n^{'} - y_p)^2 \end{aligned} \tag{7}$$

Here x_p and y_p are the coordinates of the principal point, K_1, K_2 and K_3 are the radial distortion parameters, and P_1 and P_2 are the decentering distortion parameters. A camera calibration can be used to determine the lens distortion parameters.

4.2 Approximated principal distance

The *principal distance* (*c*) of a camera in photogrammetry is defined as the distance of the perpendicular line from the *perspective center* (center of lens opening) to the image plane of the camera, which is approximated as the *focal length* (*f*) of the camera in the *collinearity equations* of Eq. (1). In this research, we seek the actual principal distance instead of the approximated camera focal length as the reconnaissance project requires the achievable level of measurement accuracy to be as high as possible.

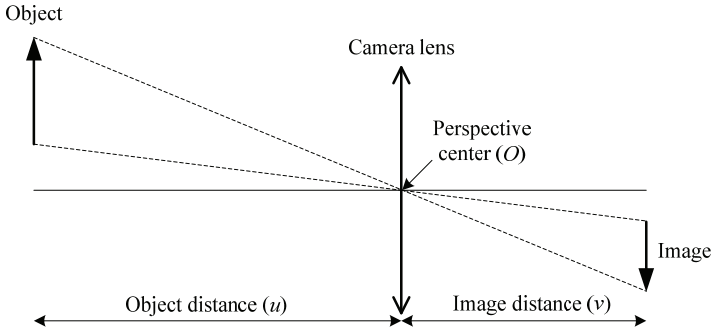

Fig. 6: Illustrated object distance and image distance when a camera is photographing an object

Fig. 6 shows a camera photographing an object where the photographic object distance and the image distance are illustrated. The principal distance *c* equals the image distance *v* when the image plane is at the exact position along the optical axis that an object is clearly focused. Meanwhile, the distance between the object and the camera lens is defined as object distance *u*. The conjugated distances *u*, *v* and the focal length *f* are related by the *lens conjugate equation* (Ray 1984) as: $1/u + 1/v = 1/f$, by which the image distance can be derived by Eq. (8):

$$v = \frac{uf}{u - f} \tag{8}$$

Eq. (8) computes the actual length of the principal distance. Also, as an object is actually shot, the object distance *u* usually is much farther than the image distance *v*. As such, the denominator (*u* - *f*) can be approximated as *u*, which yields: $v \approx f$. This proves the assertion that the *principal distance* (*c*) can be practically approximated to the focal length of the camera lens when focused at infinity, namely, $c \approx f$.

5. CAMERA CALIBRATION

5.1 Description of calibration

The calibration procedure is important for the successful implementation of this earthquake reconnaissance project, and its goal is to determine the camera's lens distortion parameters and interior parameters in terms of the fine-tuned focal length and the displacement of the principal point in a single run. The camera calibration usually involves two steps: (1) taking the calibration photos, and (2) deriving the camera parameters with those photos. Take an example of a calibrator in the well-established commercial software system – PhotoModeler® (Eos Systems Inc. 2009), which prevails both in the industrial market and in the research field. Twelve photos of a calibration grid are recommended to be taken from four edges of the grid with a combination of a portrait orientation and two landscape orientations (left and right) (PhotoModeler User's Manual 2004). The camera's focal length needs to be kept constant during the entire course of photo taking. In order to ensure that the entire lens is calibrated, the photo frames should cover as much as possible the grid dots when taking photos, and each four photos should have the grid dots align along the left, right, and top and bottom edge of the photo respectively (as illustrated in Fig. 7a). The calibration grid is a pattern of dots designed specifically for the Camera Calibrator in PhotoModeler®, and the Camera Calibrator is a computer program running on the algorithm to automate the derivation of camera parameters. Fig. 7b shows the cameras' positions and orientations when twelve photographs were exposed in PhotoModeler® as part of the camera calibration result.

(a) (b)

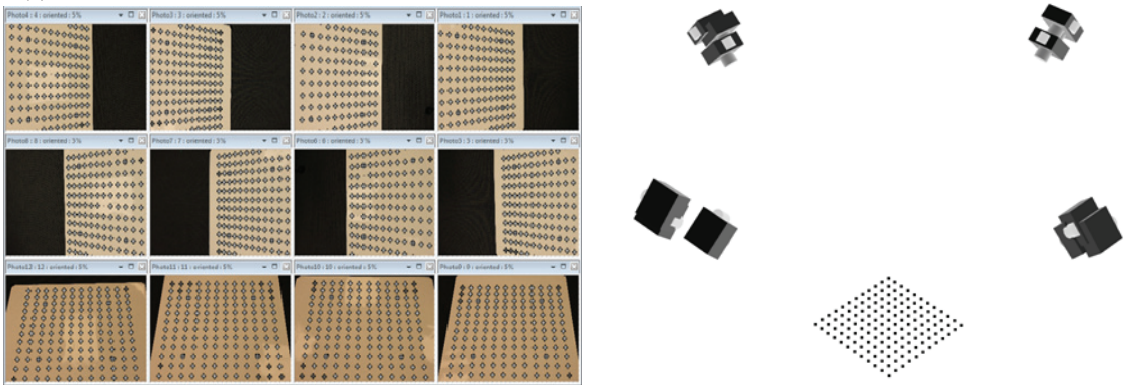

Fig. 7: Illustrated (a) calibration grid dots covered in twelve photos, and (b) twelve camera positions evaluated in PhotoModeler® as part of camera calibration result

5.2 Calibration results

The camera used to imitate the inspector's camera in this research was an off-the-shelf digital single lens reflection (DSLR) camera – Canon EOS REBEL T1i with its focal length set at 55 mm to obtain the longest shooting range of the camera. By following the calibration procedure described above, we have the calibration results for the designated camera as: the radial lens distortion parameters ($K1$ = -2.203e-005, $K2$ = -1.267e-008, $K3$ = 0), decentering lens distortion parameters ($P1$ = -1.179e-004, $P2$ = 0), the image coordinates (x_p, y_p) of the principal point (12.1573 mm, 7.7877 mm), and the adjusted focal length (f = 55.4121 mm). The threshold for evaluating the quality of calibration is that the maximum residuals are less than one pixel (PhotoModeler User's Manual 2004). In this research, this calibration yielded the maximum residuals value as 0.9191, reflecting a good calibration of the camera parameters. A residual here means the discrepancy of the distance between the calibrated each grid dot and its most likely value that is statistically calculated.

It is noteworthy that the calibration work is only needed during the first time of using the camera to take source photos. As long as the focal length doesn't change, successive modeling work can use the same calibration results to determine the internal camera parameters. The obtained camera interior parameters and lens distortion parameters will be used to calculate the undistorted coordinates of the projected image points in the experiments in order to test the validity of the proposed method, which is discussed in the next section.

6. LABORATORY EXPERIMENTS AND RESULTS

The indoor experiments were conducted in the UM Construction Laboratory to validate the feasibility of the proposed earthquake reconnaissance method. In the first phase, we primarily focused on the internal components of a digital camera that account for the measurement error. Thus, we used a tape rather than the RTK-GPS to manually measure the 3D coordinates of the camera position. Fig. 8a gives an overview of the setup for the experiment environment, in which a two storey reconfigurable steel frame was installed to mimic a building structure. The frame was calibrated with known precise displacement values at the second floor. To measure the camera's rotation angles, a 3D electronic compass was customized with a flat plate attached on the camera's hot shoe, and the angle readings were transmitted real time to a connected laptop with a data wire (Fig. 8b). The inter-storey drift between the second and third floor of the frame was studied in this experiment, and the positions of the inspected floors were denoted by two bolted connections that lie along the left edge of the frame as illustrated in Fig. 8c. Subtracting the horizontal axis components of the two connections thus helped compute the desired inter-storey drift.

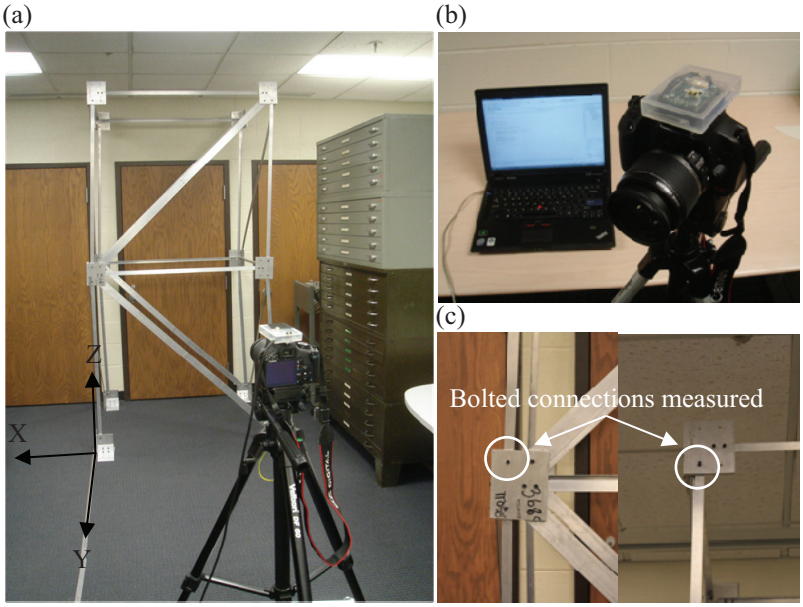

Fig. 8: (a) Experiment setup overview, (2) customized compass attached on the camera, and (3) bolted connections denoting positions of two inspected floors

The parameters for line of sight of the camera (*collinearity equations* Eq. 1) were fitted with the measured camera's coordinates and angles together with the adjusted camera focal length. For ease of computation, we simply assume that the X-axis of the global coordinate system is aligned with the horizontal movement of the inspected floors, the Z-axis is perpendicular to the ground that points upward, and the origin is at the left frontal corner of the frame (Fig. 8a). As such, the formula of plane to represent the inspected wall was obtained as $Y = 0$. Using the derived *collinearity equations* and the formula of plane, the spatial coordinates of horizontal axes for the bolted connections could be calculated from the captured images. Subsequently, the inter-storey drift could be determined.

The camera setup was as: the position coordinates (-0.489, 5.613, 1.34) m with the focal length set 55 mm. Three groups of experiments were conducted, of which each group had the camera's perspective rotated within a certain range to extensively verify the accuracy and consistency of measurements. The calibrated actual displacement was 45 mm to the left. The resulting measurements of the three experiments are presented in Table 1. The average errors for three groups of drift measurements are -5.87, -2.2, and -6.21 respectively with small standard deviations, all indicating a good level of accuracy in the proposed method.

The experimental results also reveal that the photos taken under the indoor laboratory condition (illuminated by fluorescent lamp) can have a satisfactory quality for applying photogrammetry. The camera used, which was the off-the-shelf Canon EOS REBEL T1i with the maximum resolution 15 mega pixels and autofocus functionality, is expected to take photos of even higher quality in an outdoor setting, where the reconnaissance system is genuinely utilized.

Table 1: Second-storey drifts measured using photogrammetry

	Group 1		Group 2		Group 3	
Frame No.	Drift (mm)	Error (mm)	Drift (mm)	Error (mm)	Drift (mm)	Error (mm)
1	-50.81	-5.81	-47.61	-2.61	-51.26	-6.26
2	-51.02	-6.02	-46.97	-1.97	-51.28	-6.28
3	-50.16	-5.16	-46.66	-1.66	-50.73	-5.73
4	-51.08	-6.08	-47.18	-2.18	-50.75	-5.75
5	-51.18	-6.18	-47.48	-2.48	-51.16	-6.16
6	-51.33	-6.33	-47.34	-2.34	-51.41	-6.41
7	-50.55	-5.55	-47.64	-2.64	-51.11	-6.11
8	-50.35	-5.35	-47.17	-2.17	-51.23	-6.23
9	-51.16	-6.16	-46.79	-1.79	-51.61	-6.61
10	-51.10	-6.10	-47.17	-2.17	-51.58	-6.58
Average Error (mm)		-5.87		-2.20		-6.21
Error Std Dev (mm)		0.39		0.33		0.30

7. CONCLUSIONS

This paper proposed a semi-automated method to rapidly measure structural damage induced in tall buildings by seismic events such as earthquakes or explosions by applying close-range photogrammetry surveying techniques and Augmented Reality (AR) visualization. Analytical measurement algorithms were devised, lens distortion and approximated calculation of camera focal length that account for camera systematical error were assessed, and laboratory experiments were conducted to validate measurement accuracy.

Future extension of the presented research is to implement the proposed reconnaissance system in non-laboratory outdoor conditions that real life seismic disasters reside in. External tracking Global Positioning Systems will be included to account for overall accuracy of this technique in extrapolating the inter-storey drifts. Recent advances in satellite transmission technology allow the dual-frequency GPS receivers to achieve a centimeter level of accuracy for RTK work without base station (Trimble® Vrs Now™ 2010), which promises to overcome the technical hurdle of tracking the inspector's (camera's) perspective for the proposed technique to be deployed in the field.

Another extension is an endeavor toward full automation of the reconnaissance method by looking into techniques in the research area of computer vision for direct detection of edges of key floors sustained in a damaged building on images. Preliminary study has found that the outline of a damaged building can be effectively extracted by the Active Contours technique (Caselles et al. 1997) embedded in Augmented Reality visualization. Nonetheless, the technique's validity and applicability should be further meticulously investigated.

8. ACKNOWLEDGEMENTS

This presented research was partially funded by the US National Science Foundation (NSF) under Grant CMMI-0726493. The writers gratefully acknowledge NSF's support. This research was also partially supported by the PhD student overseas exchange program of the Hong Kong Polytechnic University (PolyU). Any opinions, findings, conclusions, and recommendations expressed in this paper are those of the authors and do not necessarily reflect the views of the NSF or PolyU.

9. REFERENCES

Applied Technology Council (ATC). (1989). Procedures for postearthquake safety evaluations of buildings, *Rep. No. ATC-20*, Redwood City, Calif.

Applied Technology Council (ATC). (1995). Addendum to ATC-20: Procedures for postearthquake safety evaluations of buildings, *Rep. No. ATC-20-2*, Redwood City, Calif.

Beyer, H.A., Uffenkamp, V. and van der Vlugt, G. (1995). Quality control in industry with digital photogrammetry, *Optical 3-D Measurement Techniques III*, eds. A. Gruen and H. Kahmen, Wichmann Verlag, Heidelberg, 29-38.

Blachut, T.J. and Burkhardt, R. (1989). *Historical development of photogrammetric methods and instruments*,

ASPRS, Falls Church, VA, Chap. 1, 4-18.

Brown, D.C. (1966). Decentering distortion of lenses, *Photogrammetric Engineering*, Vol. 32, No. 3, 444-462.

Caselles, V., Kimmel, R. and Sapiro, G. (1997). Geodesic active contours, *International Journal of Computer Vision*, Vol. 22, No. 1, 61-79.

Eos Systems Inc. (2004). User Manual for PhotoModeler® Pro Version 5, Vancouver, BC.

Eos Systems Inc. (2009). PhotoModeler: Close-range photogrammetric measurement and 3D modeling software, available via <http://www.photomodeler.com> [accessed October 20, 2009].

Federal Emergency Management Agency (FEMA). (2000b). Recommended seismic design criteria for new steel moment-frame buildings, *Rep. No. 350*, Building Seismic Safety Council, Washington, D.C.

Fraser, C.S. (1996). Industrial measurement applications, *Close Range Photogrammetry and Machine Vision*, Ed. K.B. Atkinson, Whittles, Scotland, Chap. 12, 329-361.

Kamat, V.R. and El-Tawil, S. (2007). Evaluation of augmented reality for rapid assessment of earthquake-induced building damage, *Journal of Computing in Civil Engineering*, ASCE, Vol. 21, No. 5, 303-310.

McGlone, J.C. (1989). Analytic data-reduction schemes in non-topographic photogrammetry, *Non-Topographic Photogrammetry*, 2nd ed., ed. H.M. Karara, ASPRS, Falls Church, VA, Chap. 4, 37-55.

Ray, F.S. (1984). Photographic optics, *Photography for the Scientist*, 4th ed., ed. Morton, A.R., Academic Press Inc, Orlando, FL, Chap. 2, 104-124.

Trimble Navigation Limited (2010). Trimble® Vrs Now™: A real RTK network solution for GPS rover to receive high quality, location independent correction data, available via <http://www.trimble.com/vrsnow.shtml>, [accessed July 31, 2010].

Viswanathan, M. (2005). *Measurement Error and Research Design*, Sage Publications, Thousand Oaks, CA.

Wolf, P. (1983). *Elements of Photogrammetry*, McGraw-Hill, New York.

Wong, K.W. (1980). Basic mathematics of photogrammetry, *Manual of Photogrammetry*, 4th ed., ed. C.C. Slama, ASPRS, Falls Church, VA, Chap. 2, 37-101.